

Rapid Detection of Hot-spots via Tensor Decomposition with applications to Crime Rate Data

Yujie Zhao, Hao Yan, Sarah Holte, and Yajun Mei

Abstract

We propose an efficient statistical method (denoted as SSR-Tensor) to robustly and quickly detect hot-spots that are sparse and temporal-consistent in a spatial-temporal dataset through the tensor decomposition. Our main idea is to first build an SSR model to decompose the tensor data into a Smooth global trend mean, Sparse local hot-spots and Residuals. Next, tensor decomposition is utilized as follows: basis are introduced to describe within-dimension correlation and tensor products are used for between-dimension interaction. Then, a combination of LASSO and fused LASSO is used to estimate the model parameters, where an efficient recursive estimation procedure is developed based on the large-scale convex optimization, where we first transform the general LASSO optimization into regular LASSO optimization and apply FISTA to solve it with the fastest convergence rate. Finally, a CUSUM procedure is applied to detect when and where the hot-spot event occurs. We compare the performance of the proposed method in a numerical simulation and a real-world dataset, which is a collection of three types of crime rates for U.S. mainland states during the year 1965-2014. In both cases, the proposed SSR-Tensor is able to achieve the fast detection and accurate localization of the hot-spots.

Keywords: tensor decomposition, spatio-temporal, hot-spot detection, quick detection, CUSUM

1 Introduction

The objective of our research is *hot-spot* detection when monitoring multiple data sources or streams across different spatial regions over time, where one is interested in quickly and accurately determining which data sources or streams change their patterns at which local regions and at which time. A concrete motivating example is to monitor three types of annual crime rates from 1965 to 2014 for 48 mainland states in the United States, see Section 2 below for the detailed data description. There are two kinds of changes: one is at the global level, and the other is at the local level. For hot-spot detection, we are more interested in detecting those local changes with the following two properties: (1) spatial sparsity, i.e., the local changes are sparse in the spatial domain; (2) temporal persistence, i.e., the local changes last for a reasonably long time period unless one takes some actions.

Generally speaking, hot-spot detection can be thought of as change-point detection problem in spatio-temporal data. There are three different categories of methodologies and approaches in the literature. The first one is LASSO-based control chart that integrates LASSO estimators for change point detection and declares non-zero components of the LASSO estimators as the hot-spot, see Zou and Qiu (2009), Zou et al. (2012), Zou et al. (2008), Šaltytė Benth and Šaltytė (2011). Unfortunately, the LASSO-based control chart lacks the ability to separate the local hot-spots from the global trend in the spatio-temporal data. The second category of methods is the dimension-reduction-based control chart where one monitors the features from Principal Component Analysis (PCA) or other dimension reduction methods. For example, Liu (1995) reduce the dimensionality in spatio-temporal data by constructing T2 and Q charts. And Paynabar et al. (2016) combine multivariate functional PCA with change-point models to detect the hot-spots. See Paynabar et al. (2013), De Ketelaere et al. (2015), Louwerse and Smilde (2000), Hu and Yuan (2009), Bakshi (1998) for more details. The drawback of PCA or other dimension reduction based methods is the restriction of the change detection problem and the failure to take full advantage of the spatial location of hot-spot. The third category of hot-spot detection methods from spatio-temporal data is the decomposition-based method that decomposes the hot-spot from background events. For example, Yan et al. (2017) and Yan et al. (2018) proposed Smooth-Sparse Decomposition (SSD) model for hot-spot detection in the spatio-temporal

data. SSD can separate hot-spot from the functional mean by utilizing the spatial structure of both the functional mean and hot-spot. More reference can be found in Zhang et al. (2018), Yu et al. (2019), Tran et al. (2012), Yan et al. (2014), Li et al. (2019), etc.. However, these existing approaches investigate structured images or curves data and assume that the hot-spot events are independent over the time domain.

In this paper, we propose to develop a decomposition-based hot-spot detection method when the hot-spots are from autoregressive (AR) model, which is typical for time series data. Our main idea is to represent the raw data as a 3-dimensional tensor, and decompose the tensor into three components: Smooth global trend, Sparse local hot-spot, and Residuals. We term our proposed decomposition model as *SSR-Tensor*. And when fitting the raw data to the SSR-Tensor, we propose to add two penalty functions: one is the LASSO type penalty to guarantee the sparsity of hot-spots, and the other is the fused-LASSO type penalty to the autoregressive properties of a hot-spot or time-series data. Through our proposed SSR-Tensor model, we are able to (1) detect when the hot-spot happens (i.e., the change point detection problem); and (2) localize where and which type of the hot-spots occurs if the change happens (i.e., the spatial localization problem). We call the first capacity as *hot-spot detection* and the second capacity as *hot-spot localization*.

Considerable research has been done on modelling and prediction of the spatio-temporal data. Some popular time series models are AR, MA, ARMA model, etc.. And the parameters can be estimated by the Yule-Walker method (Hannan and Quinn, 1979), maximum likelihood estimation or the least squares method (Hamilton, 1994). In addition, spatial statistics have also been extensively investigated in their own right, see Reynolds and Madden (1988), Lichstein et al. (2002), Lan et al. (2004), Elhorst (2014), Call and Voss (2016). When one combines time series with spatial statistics, the corresponding spatio-temporal models generally become more complicated, see Zhu et al. (2005), Lai and Lim (2015). Also see the textbook Diggle (2013) for additional and detailed discussion. We emphasize that our proposed SSR-Tensor model is different from these existing spatio-temporal models in the sense that its primary objective is for hot-spot detection, not for estimation or prediction.

While our paper focuses only on a 3-dimensional tensor due to our motivating ap-

plication in crime rates, our proposed SSR-Tensor model can easily be extended to any d -dimensional tensor ($d \geq 3$), e.g., if we have further information, such as the unemployment rate, economic performance and so on. The reason is that our proposed model uses the *basis* to describe correlation within each dimension, and utilizes *tensor products* for interaction between different dimensions. Thus, as the dimension d increases, we just need to add the corresponding bases. The capability of extending to high-dimensional data is the main advantage of our proposed SSR-Tensor model.

The remainder of this paper is as follows. Section 2 introduces and visualizes the crime rate dataset, which is used as our motivating example. Section 3 presents our proposed SSR-Tensor model and discusses how to estimate model parameters from data. Section 4 describes how to use our proposed SSR-Tensor model to find hot-spots, both for detection and localization. Our proposed methods are validated through extensive simulations in Section 5 and the case study using the crime rate dataset is shown in Section 6.

2 Motivating Example & Background

This section gives a detailed description of the crime rate dataset used in this paper. The dataset is available from the website of the U.S. Department of Justice Federal Bureau of Investigation, see <https://www.ucrdatatool.gov/Search/Crime/State/StateCrime.cfm>. The crime rate dataset is recorded from 1965 to 2014 for 48 mainland states in U.S. annually. In each year and for each state, three types of crime rates are recorded: a) *Murder and non-negligent manslaughter*; b) *Legacy rape*; and c) *Revised rape*. These three annual crime rates are denoted by r_1 , r_2 and r_3 , respectively.

It is worth noting that, our motivating dataset is of three dimensions, which includes the year (temporal dimension), state (spatial dimension) and different types of crime rates (category dimension). For the purpose of clarity and visual representation, we plot several figures which shows the characteristic of each dimension. To begin with, we first show the characteristic of the temporal domain (year), where we plot the time series of the annual crime rate for the entire U.S. in Figure 1(a). The x-axis is the year ranging from 1965 to 2014, and the y-axis is the annual crime rate of U.S.. It can be seen that, the crime rates are increasing in the first ten years during 1965-1975, then become stationary during

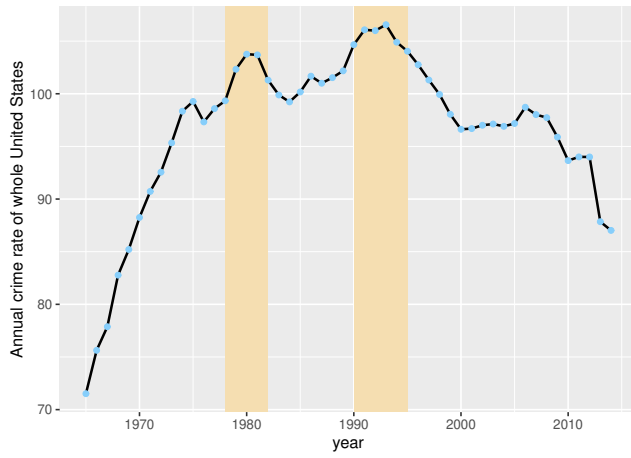
1975-1995, and finally have a decreasing trend during 1995-2014. And we also highlight the two peaks around 1980 and 1992 as well.

Then we show the characteristic of our motivating data on the category domain (type of the crime rates) in Figure 1(b), where different bars represents different type of the crime rates, and the height of the bar represents the cumulative crime rate from 1965 to 2014. It can be seen that, these three crime rates overall performs similarly, which makes it different to detect the hot-spot if we compress the three-dimension data into one dimension only.

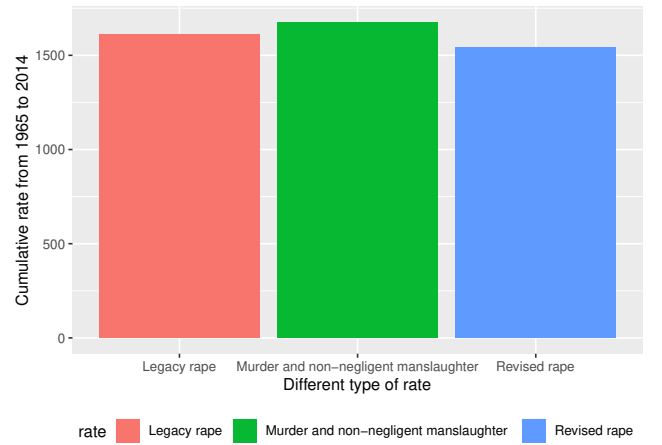
Finally, we show the characteristic of our motivating data on the spatial domain (state) in Figure 2. In Figure 2, each map shows the spatial information of the third crime rate (revised rape) in six different years. And the selected six years is starting from 1965, and ranging with a ten-year interval. For the sixth map, since the data in Year 2015 is not available yet, we use Year 2014 instead. We can see from the spatial plot in Figure 2 that the crime rate spatial patterns are different in different years. In addition, the crime rates are increasing in the first ten years and are decreasing in the last ten years, which is consistent with that in Figure 1(a).

From Figure 1 and Figure 2, there seems to have a brief increasing trend during 1984-1995, but it is difficult to visually conclude whether this is due to the global change or local hot-spots without refined analysis. If this is a local hot-spot event, we want to detect when the hot-spot appears, and then identify where and which type of crime rate accounts for this change. Since the data have three dimensions (states, rates and year), how to properly model the global trend and local hot-spot structures become very crucial, which is the motivation for our proposed model described in Section 3.1.

It is worth noting that, we store our data as a three-dimension tensor, and we noted it as \mathcal{Y} . Mathematically speaking, the element $\mathcal{Y}_{i,j,t}$ represents the j -th crime rate of state i in year t , where $i = 1, \dots, 48$ for 48 mainland states, $j = 1, \dots, 3$ for three different type of crime rate and $t = 1, \dots, 50$ for 50 years from 1965 to 2014. And in our data analysis in the next sections, we will model this multi-dimensional array through tensor decomposition. For the convenience of notation and ease of understanding, we first introduce some basic tensor algebra and notation, including basic notation, definitions, and operators in tensor (multi-linear) algebra that are useful in this paper. Throughout the paper, scalars

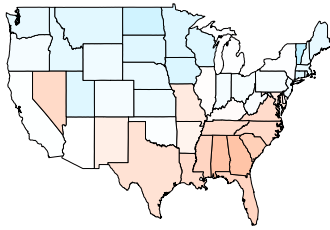


(a) Time Series plot

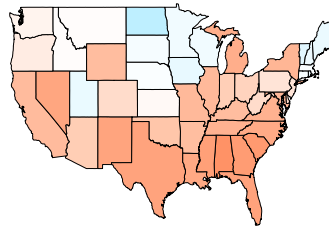


(b) Bar plot

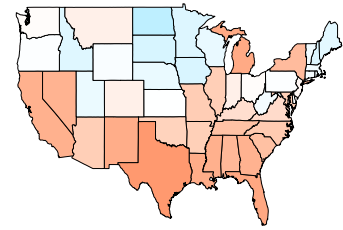
Figure 1: Time Series of Annual Crime Rates in the US over the 50 years during 1965-2014 (left) & Bar plot of three cumulative rates from 1965 to 2014 (right)



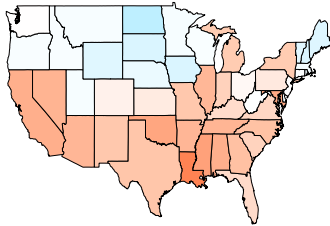
(a) 1965



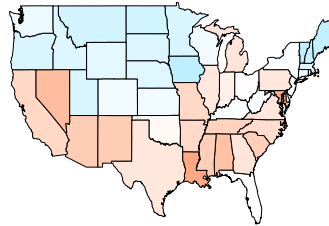
(b) 1975



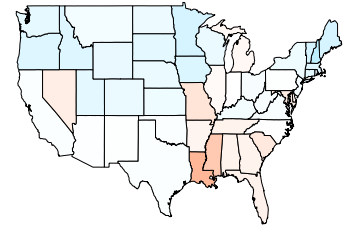
(c) 1985



(d) 1995



(e) 2005



(f) 2014

Figure 2: Raw Data for the the third type of crime rate (r_3) in six different years. From left to right, the top row represents Year 1965, 1975 and 1985, whereas the bottom row are from Year 1995, 2005 and 2014. The red means high crime rates, whereas the blue implies low crime rates.

are denoted by lowercase italic letters (e.g., θ), vectors by lowercase boldface letters ($\boldsymbol{\theta}$), matrices by uppercase boldface letter ($\boldsymbol{\Theta}$), and tensors by curlicue letter (ϑ). For example, an order- K tensor is represented by $\vartheta \in \mathbb{R}^{I_1 \times \dots \times I_K}$, where I_k represents the mode- k dimension of ϑ . The mode- k product of a tensor ϑ by a matrix $\mathbf{B} \in \mathbb{R}^{P_k \times I_k}$ is defined by $(\vartheta \times_k \mathbf{B})(i_1, \dots, i_{n-1}, j_k, i_{n+1}, \dots, i_N) = \sum_{i_k} \boldsymbol{\Theta}(i_1, \dots, i_k, \dots, i_N) \mathbf{B}(j_k, i_k)$. The n -mode unfolds maps in the tensor ϑ into matrix $\boldsymbol{\Theta}_{(n)}$, where the column of $\boldsymbol{\Theta}_{(n)}$ are the n -mode vectors of ϑ .

A very useful technique in tensor algebra is the Tucker decomposition, which decomposes a tensor into a core tensor multiplied by a matrix along each mode: $\mathcal{Y} = \vartheta \times_1 \mathbf{B}^{(1)} \times_2 \mathbf{B}^{(2)} \dots \times_K \mathbf{B}^{(K)}$, where $\mathbf{B}^{(k)}$ is an orthogonal $I_k \times I_k$ matrix and is a principal component mode- k . Tensor product can be represented equivalently by a Kronecker product, i.e., $\text{vec}(\mathcal{Y}) = (\mathbf{B}^{(K)} \otimes \dots \otimes \mathbf{B}^{(1)}) \text{vec}(\boldsymbol{\Theta})$, where vec is the vectorized operator defined as $\text{vec}(\mathcal{Y}) = \mathcal{Y}_{(K+1)}$ (an $I_1 \times I_2 \times \dots \times I_K$ -dimension vector). The definition of Kronecker product is as follow: Suppose $\mathbf{B}_1 \in \mathbb{R}^{m \times n}$ and $\mathbf{B}_2 \in \mathbb{R}^{p \times q}$ are matrices, the Kronecker product of these matrices, denoted by $\mathbf{B}_1 \otimes \mathbf{B}_2$, is an $mq \times nq$ block matrix defined by

$$\mathbf{B}_1 \otimes \mathbf{B}_2 = \begin{bmatrix} b_{11}\mathbf{B}_2 & \dots & b_{1n}\mathbf{B}_2 \\ \vdots & \ddots & \vdots \\ b_{m1}\mathbf{B}_2 & \dots & b_{mn}\mathbf{B}_2 \end{bmatrix}.$$

3 Our Proposed SSR-Tensor Model

This section presents our proposed methodology. Owing to the fact that the crime rate data is of three dimensions, namely states, rates and year, it will likely have complex within-dimension and between-dimension relationships. A within-dimension relationship includes within-state correlation, within-crime-type correlation, and within-year correlation. Between-dimension correlations include between-state-and-crime-type interaction, between-state-and-year interaction, as well as between-year-and-crime-type interaction. In order to handle these complex “within-dimension” and “between-dimension” interaction structures, we use the tensor decomposition method, where basis are used to address “within” correlation, and the tensor product is used for “between” interaction. Choice of basis is a very important concept since different basis can be chosen for different di-

mensions. Mathematically speaking, basis are a matrix which describes the structure of its corresponding dimension, and tensor products are an operator in tensor algebra. The detailed discussion on the selection of basis is developed in Section 3.3.

The structure of this section is that, Section 3.1 presents our proposed model that is able to characterize the complex correlation structures. Section 3.2 develops the optimization algorithm to solve the estimation problem in Section 3.1. And Section 3.3 discusses the choice of basis in practice.

3.1 Our Proposed Model

Our proposed model is built on tensors of order three, as it applies to the crime rate dataset which has three components and can be represented as a three dimension tensor $\mathcal{Y}_{n_1 \times n_2 \times T}$ with $n_1 = 48$ mainland states, $n_2 = 3$ different types of crime rates, and $T = 50$ years.

Note that the i^{th}, j^{th} , and k^{th} slice of the 3-D tensor along the dimension of state, crime type, and year can be achieved as $\mathcal{Y}_{i::}, \mathcal{Y}_{:j:}, \mathcal{Y}_{::k}$ correspondingly, where $i = 1 \dots n_1$, $j = 1 \dots n_2$ and $k = 1 \dots T$. For simplicity, we denote $\mathbf{Y}_k = \mathcal{Y}_{::k}$. We further denote \mathbf{y}_k as the vectorized form of \mathbf{Y}_k , and \mathbf{y} as the vectorized form of \mathcal{Y} .

The key idea of our proposed model is to separate the global trend from the local pattern by decomposing the tensor \mathbf{y} into three parts, namely the smooth global trend $\boldsymbol{\mu}$, local hot-spots \mathbf{h} , and residuals \mathbf{e} , i.e. $\mathbf{y} = \boldsymbol{\mu} + \mathbf{h} + \mathbf{e}$. For the first two of the components (e.g. the global time trend mean and local hot-spots), we introduce basis decomposition framework to represent the structure of the within correlation in the global background and local hot-spots, also see Yan et al. (2018).

To be more concrete, we assume that global trend mean and local hot-spots can be represented as $\boldsymbol{\mu} = \mathbf{B}_m \boldsymbol{\theta}_m$ and $\mathbf{h} = \mathbf{B}_h \boldsymbol{\theta}_h$, where \mathbf{B}_m and \mathbf{B}_h are two bases that will be discussed below. The vectors $\boldsymbol{\theta}_m$ and $\boldsymbol{\theta}_h$ are the model coefficients vector of length $n_1 n_2 T$ and needed to be estimated, and we will discuss the estimation method later. Here the subscript of m and h are abbreviations for the mean and hot-spots. Since the first parameter $\boldsymbol{\theta}_m$ is to estimate the global trend mean, and we refer it as *global mean parameter*. And the second parameter $\boldsymbol{\theta}_h$ is to estimate the local hot-spots, and we call it as *local hot-spots parameter*.

It is useful to discuss how to choose the bases \mathbf{B}_m and \mathbf{B}_h , so as to characterize the complex “within” and “between” correlation or interaction structures. For the “within” correlation structures, we propose to use pre-specified bases, $\mathbf{B}_{m,s}$ and $\mathbf{B}_{h,s}$, for within-state correlation in global trend and hot-spot, where the subscript of s is an abbreviation for states. Similarly, $\mathbf{B}_{m,r}$ and $\mathbf{B}_{h,r}$ are the pre-specified bases for within-correlation of the same type of crime rates, whereas $\mathbf{B}_{m,t}$ and $\mathbf{B}_{h,t}$ are the bases for within-year correlation over time. As for the “between” interaction, we use a tensor product to describe this interaction, i.e, $\mathbf{B}_m = \mathbf{B}_{m,s} \otimes \mathbf{B}_{m,r} \otimes \mathbf{B}_{m,t}$ and $\mathbf{B}_h = \mathbf{B}_{h,s} \otimes \mathbf{B}_{h,r} \otimes \mathbf{B}_{h,t}$. This Kronecker product has been proved to have better computational efficiency in the tensor response data (Kolda and Bader, 2009). With the well-structured “within” and “between” interaction, our proposed model can be written as:

$$\mathbf{y} = (\mathbf{B}_{m,s} \otimes \mathbf{B}_{m,r} \otimes \mathbf{B}_{m,t})\boldsymbol{\theta}_m + (\mathbf{B}_{h,s} \otimes \mathbf{B}_{h,r} \otimes \mathbf{B}_{h,t})\boldsymbol{\theta}_h + \mathbf{e}, \quad (1)$$

where $\mathbf{e} \sim N(0, \sigma^2 \mathbf{I})$ is the random noise. Mathematically speaking, both $\mathbf{B}_{m,s}$ and $\mathbf{B}_{h,s}$ are $n_1 \times n_1$ matrix, $\mathbf{B}_{m,r}$ and $\mathbf{B}_{h,r}$ are $n_2 \times n_2$ matrix and $\mathbf{B}_{m,t}$ and $\mathbf{B}_{h,t}$ are $n_T \times n_T$ matrix, respectively. Besides, our proposed model in (1) can also be rewritten into a tensor format:

$$\mathcal{Y} = \vartheta_m \times_3 \mathbf{B}_{m,t} \times_2 \mathbf{B}_{m,r} \times_1 \mathbf{B}_{m,s} + \vartheta_h \times_3 \mathbf{B}_{h,t} \times_2 \mathbf{B}_{h,r} \times_1 \mathbf{B}_{h,s} + \mathbf{e}, \quad (2)$$

where ϑ_m and ϑ_h is the tensor format of $\boldsymbol{\theta}_m$ and $\boldsymbol{\theta}_h$ with dimensional $n_1 \times n_2 \times n_T$. Accordingly, the $(i, j, t)^{th}$ element in ϑ_m, ϑ_h (or equivalently the $((k-1)n_1n_2 + (i-1)n_1 + j)^{th}$ entry of $\boldsymbol{\theta}_h, \boldsymbol{\theta}_m$) can estimate the global mean and hot-spots in the i^{th} state and j^{th} crime rate in k^{th} year respectively. The tensor representation in equation (2) allows us to develop computationally efficient methods for estimation and prediction.

After developing the models above in equation (1), we now discuss how to estimate the parameters $\boldsymbol{\theta}$ s (the global mean parameter $\boldsymbol{\theta}_m$ and the local hot-spots parameter $\boldsymbol{\theta}_h$) in our model from the data via the penalized likelihood function. We propose to add two penalties in our estimation. First, because hot-spots rarely occur, we assume that the local hot-spots parameter $\boldsymbol{\theta}_h$ is sparse and the majority of entries in the hot-spot coefficient $\boldsymbol{\theta}_h$ are zeros. Thus, we propose to add the penalty term $R_1(\boldsymbol{\theta}_h) = \lambda \|\boldsymbol{\theta}_h\|_1$ to encourage the sparsity property of $\boldsymbol{\theta}_h$. Second, we assume there is temporal continuity of the hot-spots, as the unusual phenomenon of last year is likely to affect the performance of hot-spots in

the current year. Thus, we add the second penalty $R_2(\boldsymbol{\theta}_h) = \lambda_2 \sum_{t=2}^T \|\boldsymbol{\theta}_{h,t} - \boldsymbol{\theta}_{h,t-1}\|_1$ to ensure the temporal continuity of the hot-spot, where $\boldsymbol{\theta}_{h,t}$ is a sub-vector of length $n_1 n_2$ starting from the $((t-1)n_1 n_2 + 1)^{th}$ element to the $(tn_1 n_2)^{th}$ element in $\boldsymbol{\theta}_h$, which represents the hot-spot parameter for the t^{th} year. By combining both two penalties, we propose to estimate the parameters $(\boldsymbol{\theta}_m, \boldsymbol{\theta}_h)$ via the following optimization problem:

$$\begin{aligned} \arg \min_{\boldsymbol{\theta}_m, \boldsymbol{\theta}_h} \|\mathbf{e}\|^2 + \lambda_1 \|\boldsymbol{\theta}_h\|_1 + \lambda_2 \sum_{t=2}^T \|\boldsymbol{\theta}_{h,t} - \boldsymbol{\theta}_{h,t-1}\|_1 \\ s.t. \quad \mathbf{y} = (\mathbf{B}_{m,s} \otimes \mathbf{B}_{m,r} \otimes \mathbf{B}_{m,t})\boldsymbol{\theta}_m + (\mathbf{B}_{h,s} \otimes \mathbf{B}_{h,r} \otimes \mathbf{B}_h)\boldsymbol{\theta}_h + \mathbf{e}, \end{aligned} \quad (3)$$

where $\boldsymbol{\theta}_m = \text{vec}(\boldsymbol{\theta}_{m,1}, \dots, \boldsymbol{\theta}_{m,T})$ and $\boldsymbol{\theta}_h = \text{vec}(\boldsymbol{\theta}_{h,1}, \dots, \boldsymbol{\theta}_{h,T})$. Combining these two penalties in equation (3), we get $R(\boldsymbol{\theta}_h) = R_1(\boldsymbol{\theta}_h) + R_2(\boldsymbol{\theta}_h) = \lambda_1 \|\boldsymbol{\theta}_h\|_1 + \lambda_2 \sum_{t=2}^T \|\boldsymbol{\theta}_{h,t} - \boldsymbol{\theta}_{h,t-1}\|_1$, which is a fused LASSO penalty (Tibshirani et al., 2005) controlling both the sparsity and temporal consistency of the hot-spots. We will discuss how to efficiently optimize equation (3) for tensors in Section 3.2.

3.2 Optimization Algorithm for Estimation

In this section, we develop an efficient optimization algorithm for solving the optimization problem in equation (3). For notation convenience, we slightly adjust the notation above. Because $\boldsymbol{\theta}_m, \boldsymbol{\theta}_h$ in equation (3) is solved under penalty $\lambda_1 R_1(\boldsymbol{\theta}_h) + \lambda_2 R_2(\boldsymbol{\theta}_h)$, we re-denote $\boldsymbol{\theta}_m, \boldsymbol{\theta}_h$ as $\boldsymbol{\theta}_{m,\lambda_1,\lambda_2}, \boldsymbol{\theta}_{h,\lambda_1,\lambda_2}$ to emphasis the penalty parameter λ_1 and λ_2 . Accordingly, $\boldsymbol{\theta}_{h,0,\lambda_2}$ refers to the estimator only under the second penalty $\lambda_2 R_2(\boldsymbol{\theta}_h)$, i.e.,

$$\boldsymbol{\theta}_{h,0,\lambda_2} = \arg \min_{\boldsymbol{\theta}_m, \boldsymbol{\theta}_h} \{\|\mathbf{e}\|_2^2 + \lambda R_2(\boldsymbol{\theta}_h)\}. \quad (4)$$

The main idea of our proposed estimation algorithm can be summarized as follows. First we reduce the number of unknown vectors in our model, i.e, find a closed-form correlation between $\boldsymbol{\theta}_{m,\lambda_1,\lambda_2}$ given $\boldsymbol{\theta}_{h,\lambda_1,\lambda_2}$. After reducing the number of parameters, we focus on estimating $\boldsymbol{\theta}_{h,0,\lambda_2}$, where FISTA (Beck and Teboulle, 2009) is the main tool in this stage. We use notation $\hat{\boldsymbol{\theta}}_{h,0,\lambda_2}$ to describe the corresponding estimator of $\boldsymbol{\theta}_{h,0,\lambda_2}$. Finally, the estimated $\boldsymbol{\theta}_{h,\lambda_1,\lambda_2}$, described by $\hat{\boldsymbol{\theta}}_{h,\lambda_1,\lambda_2}$, is solved by the closed-form of $\hat{\boldsymbol{\theta}}_{h,\lambda_1,\lambda_2}$ given $\hat{\boldsymbol{\theta}}_{h,0,\lambda_2}$.

Following the main idea above, we first reduce the number of unknown vectors. Although there are two sets of parameters, namely $\boldsymbol{\theta}_{m,\lambda_1,\lambda_2}$ and $\boldsymbol{\theta}_{h,\lambda_1,\lambda_2}$ in the model, we note

that given $\boldsymbol{\theta}_{h,\lambda_1,\lambda_2}$, the parameter $\boldsymbol{\theta}_{m,\lambda_1,\lambda_2}$ is involved in the standard least squared estimation and thus can be solved in the closed-form solution, see equation (5) in the proposition below.

Proposition 1. In the optimization problem shown in equation (3), when given $\boldsymbol{\theta}_{h,\lambda_1,\lambda_2}$, the closed-form solution of $\boldsymbol{\theta}_{m,\lambda_1,\lambda_2}$ is given by:

$$\boldsymbol{\theta}_{m,\lambda_1,\lambda_2} = (\mathbf{B}'_m \mathbf{B}_m)^{-1} (\mathbf{B}'_m \mathbf{y} - \mathbf{B}'_m \mathbf{B}_h \boldsymbol{\theta}_{h,\lambda_1,\lambda_2}). \quad (5)$$

To estimate the parameter $\boldsymbol{\theta}_{h,\lambda_1,\lambda_2}$, we plug equation (5) into equation (3). Then, the optimization problem for estimating $\boldsymbol{\theta}_{h,\lambda_1,\lambda_2}$ in equation (3) becomes

$$\arg \min_{\boldsymbol{\theta}_{h,\lambda_1,\lambda_2}} \|\mathbf{y}^* - \mathbf{X}\boldsymbol{\theta}_{h,\lambda_1,\lambda_2}\|_2^2 + \lambda_1 \|\boldsymbol{\theta}_{h,\lambda_1,\lambda_2}\|_1 + \lambda_2 \sum_{t=2}^T \|\boldsymbol{\theta}_{h,t,\lambda_1,\lambda_2} - \boldsymbol{\theta}_{h,t-1,\lambda_1,\lambda_2}\|_1, \quad (6)$$

where $\mathbf{y}^* = [\mathbf{I} - \mathbf{H}_m] \mathbf{y}$, $\mathbf{X} = [\mathbf{I} - \mathbf{H}_m] \mathbf{B}_h$ and $\mathbf{H}_m = \mathbf{B}_m (\mathbf{B}'_m \mathbf{B}_m)^{-1} \mathbf{B}'_m$ is the projection matrix. Because solving the inverse of a matrix $\mathbf{B}'_m \mathbf{B}_m$ is computational expensive, therefore, in order to simply the calculation, we developed the tensor format of \mathbf{y}^* , which can be rewritten as $\mathbf{y}^* = \mathbf{y} - \text{vec}(\mathcal{Y} \times_1 \mathbf{H}_{m,s} \times_2 \mathbf{H}_{m,r} \times_3 \mathbf{H}_{m,t})$, where $\times_k (k = 1, 2, 3)$ is the mode- k product in Section 2 and $\text{vec}(\cdot)$ is an operator to transform variable to vectors. And $\mathbf{H}_{m,s} = \mathbf{B}_{m,s} (\mathbf{B}'_{m,s} \mathbf{B}_{m,s})^{-1} \mathbf{B}'_{m,s}$, $\mathbf{H}_{m,r} = \mathbf{B}_{m,r} (\mathbf{B}'_{m,r} \mathbf{B}_{m,r})^{-1} \mathbf{B}'_{m,r}$, and $\mathbf{H}_{m,t} = \mathbf{B}_{m,t} (\mathbf{B}'_{m,t} \mathbf{B}_{m,t})^{-1} \mathbf{B}'_{m,t}$. The details of the proof are shown in Appendix 8.1.

Due to the potential for very high dimensional data, we need to develop an efficient and precise optimization algorithm to optimize solutions to solve the global optimum of equation (3). To save computational efforts, we first solve $\boldsymbol{\theta}_{h,0,\lambda_2}$, i.e., with the sparsity penalty parameter $\lambda_1 = 0$, which is used to solve $\boldsymbol{\theta}_{h,\lambda_1,\lambda_2}$ for the general λ_1 later. The estimation of $\boldsymbol{\theta}_{h,0,\lambda_2}$ is to optimize

$$\arg \min_{\boldsymbol{\theta}_{h,0,\lambda_2}} \|\mathbf{y}^* - \mathbf{X}\boldsymbol{\theta}_{h,0,\lambda_2}\|_2^2 + \lambda_2 \|\mathbf{D}\boldsymbol{\theta}_{h,0,\lambda_2}\|_1, \quad (7)$$

where matrix \mathbf{D} is of dimension $n_1 n_2 (n_3 - 1) \times n_1 n_2 n_3$, whose $(i, i)^{th}$, $(i, i + n_1 n_2 - 1)^{th}$ elements are of value -1 and 1 , respectively.

Obviously, the optimization problem for equation (7) is a generalized LASSO problem, which can be transformed into a regular LASSO problem (Tibshirani et al., 2011). The details of the transformation procedure are shown in Proposition 2.

Proposition 2. Assume that

1. matrix \mathbf{A} is of dimension $n_1 n_2 \times n_1 n_2 n_3$ and constructed through combining $n_1 n_2 \times n_1 n_2$ identity matrix rowly $n_3 - 1$ times,
2. matrix $\tilde{\mathbf{D}}$ of dimension $n_1 n_2 n_3 \times n_1 n_2 n_3$ and is defined as $\tilde{\mathbf{D}} = \begin{bmatrix} \mathbf{D} \\ \mathbf{A} \end{bmatrix}$,
3. matrix \mathbf{X}_1 is the first $n_1 n_2 (T - 1)$ rows of matrix $\mathbf{X} \tilde{\mathbf{D}}^{-1}$, matrix \mathbf{X}_2 is the remaining part of matrix $\mathbf{X} \tilde{\mathbf{D}}^{-1}$,
4. the projection onto the column space of \mathbf{X}_2 is noted as $\mathbf{P} = \mathbf{X}_2 (\mathbf{X}_2' \mathbf{X}_2)^{-1} \mathbf{X}_2'$,
5. the first $n_1 n_2 (n_3 - 1)$ entries of $\boldsymbol{\beta}$ ($\boldsymbol{\beta} = \tilde{\mathbf{D}} \boldsymbol{\theta}_{h,0,\lambda_2}$ is noted as $\boldsymbol{\beta}_1$, and the remaining are noted as $\boldsymbol{\beta}_2$.

The generalized LASSO problem in equation (7) can be solved by $\hat{\boldsymbol{\theta}}_{h,0,\lambda_2} = \tilde{\mathbf{D}}^{-1} \hat{\boldsymbol{\beta}}$, where $\hat{\boldsymbol{\beta}} = (\hat{\boldsymbol{\beta}}_1, \hat{\boldsymbol{\beta}}_2)$ and

$$\begin{aligned} \hat{\boldsymbol{\beta}}_1 &= \arg \min_{\boldsymbol{\beta}_1} \|(\mathbf{I} - \mathbf{P}) \mathbf{y}^* - (\mathbf{I} - \mathbf{P}) \mathbf{X}_1 \boldsymbol{\beta}_1\|_2^2 + \lambda_2 \|\boldsymbol{\beta}_1\|_1 \\ \hat{\boldsymbol{\beta}}_2 &= (\mathbf{X}_2' \mathbf{X}_2)^{-1} \mathbf{X}_2' (\mathbf{y}^* - \mathbf{X}_1 \hat{\boldsymbol{\beta}}_1). \end{aligned} \quad (8)$$

Proposition 2 allows us to focus on efficiently solving the LASSO-type optimization problem in (8). To do so, we propose to use the FISTA algorithm in Beck and Teboulle (2009) due to its fast convergence rate. Indeed, Beck and Teboulle (2009) showed that the convergence rate of the FISTA algorithm is of order $O(1/k^2)$ where k indicates the iterations. And FISTA is an very efficient and standardized algorithm in optimization research to solve optimization problem involving ℓ_1 penalty. The proof of Proposition 2 can be found in Appendix 8.2.

Finally, with the solved $\hat{\boldsymbol{\theta}}_{h,0,\lambda_2}$ for $\lambda_1 = 0$, we can easily compute $\hat{\boldsymbol{\theta}}_{h,\lambda_1,\lambda_2}$ for general $\lambda_1 > 0$ due to the their closed form relations in the following proposition:

Proposition 3. The closed form relationship between $\hat{\boldsymbol{\theta}}_{h,\lambda_1,\lambda_2}$ and $\hat{\boldsymbol{\theta}}_{h,0,\lambda_2}$ is

$$\hat{\boldsymbol{\theta}}_{h,\lambda_1,\lambda_2} = \text{sign}(\hat{\boldsymbol{\theta}}_{h,0,\lambda_2}) \odot \max\{|\hat{\boldsymbol{\theta}}_{h,0,\lambda_2}| - \lambda_1, 0\}. \quad (9)$$

where \odot is an element-wise product operator.

The proof of Proposition 3 could be found in the proof of Theorem 1 of Liu et al. (2010). In summary, the details of our proposed optimization algorithm are shown in Algorithm 1 below.

Algorithm 1: Estimation of $\boldsymbol{\theta}_{h,\lambda_1,\lambda_2}$

Input: $\mathbf{y}, \mathbf{B}_{m,s}, \mathbf{B}_{m,r}, \mathbf{B}_{m,t}, \mathbf{B}_{h,s}, \mathbf{B}_{h,r}, \mathbf{B}_{h,t}, \mathbf{X}_1, \mathbf{X}_2, \tilde{\mathbf{X}} = (\mathbf{I} - \mathbf{P})\mathbf{X}_1, \tilde{\mathbf{y}} = (\mathbf{I} - \mathbf{P})\mathbf{y}^*, \lambda_1, \lambda_2, K$

Output: $\hat{\boldsymbol{\theta}}_{h,\lambda_1,\lambda_2}$

1 **initialization;**

2 $\boldsymbol{\beta}_1^{(0)}, \boldsymbol{\alpha}^{(1)} = \boldsymbol{\beta}_1^{(0)}, t_1 = 1, k = 0$

3 **for** $k = 1 \cdots K$ **do**

4 $\boldsymbol{\beta}_1^{(k)} = S\left(\boldsymbol{\alpha}^{(k)} - \frac{1}{nL} \left(\tilde{\mathbf{X}}' \tilde{\mathbf{X}} \boldsymbol{\alpha}^{(k)} + \tilde{\mathbf{X}}' \tilde{\mathbf{y}}\right), \lambda_2/L\right)$

 /* $S(\cdot)$ is the soft-thresholding function. */

5 $t_{k+1} = \frac{1 + \sqrt{1 + 4t_k^2}}{2}$

6 $\boldsymbol{\alpha}^{(k+1)} = \boldsymbol{\beta}^{(k)} + \frac{t_k - 1}{t_{k+1}} \left(\boldsymbol{\beta}^{(k)} - \boldsymbol{\beta}^{(k-1)}\right)$

7 $k = k + 1$

8 **end**

9 $\hat{\boldsymbol{\beta}}_2 = (\mathbf{X}_2' \mathbf{X}_2)^{-1} \mathbf{X}_2' (\mathbf{y} - \mathbf{X}_1 \boldsymbol{\beta}_1^{(K)})$

10 $\hat{\boldsymbol{\theta}}_{h,0,\lambda_2} = \tilde{\mathbf{D}}^{-1}(\boldsymbol{\beta}_1^{(K)}, \hat{\boldsymbol{\beta}}_2)'$

11 $\hat{\boldsymbol{\theta}}_{h,\lambda_1,\lambda_2} = \text{sign}(\hat{\boldsymbol{\theta}}_{h,0,\lambda_2}) \odot \max\{|\hat{\boldsymbol{\theta}}_{h,0,\lambda_2}| - \lambda_1, 0\}$

3.3 Selection of Bases in Practice

This section discusses how to choose a proper bases $\mathbf{B}_{m,s}, \mathbf{B}_{m,r}, \mathbf{B}_{m,t}, \mathbf{B}_{h,s}, \mathbf{B}_{h,r}, \mathbf{B}_{h,t}$. Generally speaking, some reasonable choices of the bases can be: (1) identity matrix when one has little to no prior knowledge of the data structure; (2) Gaussian kernel if the data shares a very smooth background; (3) Other kernels, including Cosine, Silverman and etc., depending on the nature or characteristics of the data.

In the crime rate data, we begin with the basis for the global trend. Figure 2 shows that the global pattern is very smooth, where no distinctive abrupt changes between neighbor states. To model the smooth spatial correlation of the global state pattern, we propose to apply kernel matrix, defined as $\mathbf{B}_{m,s}$ with $\exp\{-d^2/(2c^2)\}$ for the $(i, j)^{th}$ element, where

d is the distance between the i^{th} state and j^{th} state, and c is the bandwidth chosen by cross-validation. For the correlation among the crime rates, we set $\mathbf{B}_{m,r}$ to be an identity matrix, since we do not have any prior knowledge of it. Next, for the bases for the hot-spots, we assume there is no prior knowledge of the hot-spots. Thus we set $\mathbf{B}_{h,s}$ and $\mathbf{B}_{h,r}$ to be an identity matrix. Moreover, for the temporal basis in both global trend and hot-spots, the identity matrix is used, while this reflects that we do not know when hot-spots will occur. Our optimization algorithm includes an autoregressive-type regularization term in the estimation procedure to guarantee that there is the temporal continuity of hot-spot.

4 Detection and Localization of Hot-spots

This section focuses on the detection of a hot-spot, which includes the detection of the year (when), the state (where) as well as the crime type (which) of the hot-spot. In our case study, we focus on the upward shift of crime rates, since the increasing crime rates are generally more harmful to the societies and communities. Of course, one can also detect the downward shift with a slight modification of our proposed algorithms by multiplying -1 to the raw data.

For ease of presentation, we first discuss the detection of the hot-spot, i.e., detect when a hot-spot occurs in Section 4.1. Then, in Section 4.2, we consider the localization of the hot-spot, i.e., determine which states and which crime types are involved for the detected hot-spot.

4.1 Detect When the Hot Spot Occurs?

To determine when the hot-spot occurs, we consider the following hypothesis test and set up the control chart for the hot-spot detection in equation (10).

$$H_0 : \mathbf{r}_t = 0 \quad v.s. \quad H_1 : \mathbf{r}_t = \delta \hat{\mathbf{h}}_t \quad (\delta > 0), \quad (10)$$

where \mathbf{r}_t is the expected residuals after removing the mean. The essence of this test is that, we want to detect whether \mathbf{r}_t has a mean shift in the direction of $\hat{\mathbf{h}}_t$ (estimated in Section 3.2). Please note that $\hat{\mathbf{h}}_t$ is the subvector of $\hat{\mathbf{h}}$, starting from the $((t-1)n_1n_2+1)^{th}$ element to the $(n_1n_2t)^{th}$ element. And $\hat{\mathbf{h}}$ is derived by $\hat{\mathbf{h}} = \mathbf{B}_h \boldsymbol{\theta}_h$.

To test this hypotheses, the likelihood ratio test is applied to the residual \mathbf{r}_t at each time t , i.e. $\mathbf{r}_t = \mathbf{y}_t - \boldsymbol{\mu}_t$, where it assumes that the residuals \mathbf{r}_t is independent after removing the mean and its distribution before and after the hot-spot remains the same. Accordingly, the test statistics monitoring upward shift is designed as $P_t^+ = \widehat{\mathbf{h}}_t'^+ \mathbf{r}_t / \sqrt{\widehat{\mathbf{h}}_t'^+ \widehat{\mathbf{h}}_t^+}$ (Hawkins, 1993), where $\widehat{\mathbf{h}}_t^+$ only takes the positive part of $\widehat{\mathbf{h}}_t$ with other entries as zero. Here we put a superscript “+” to emphasis that it aims for upward shift.

Unfortunately, different choices of the penalty parameters λ_1, λ_2 gives different test statistics P_t^+ . In order to select the one with the most power, we propose to calculate a series of P_t^+ under different combination of (λ_1, λ_2) from the set $\Gamma = \{(\lambda_1^{(1)}, \lambda_2^{(1)}) \cdots (\lambda_1^{(n_\lambda)}, \lambda_2^{(n_\lambda)})\}$. For better illustration, we denote the test statistics under the penalty parameters (λ_1, λ_2) as $P_t^+(\lambda_1, \lambda_2)$. The test statistics (Zou and Qiu, 2009) with the most power to detect the change, noted as \tilde{P}_t^+ , can be computed by

$$\tilde{P}_t^+ = \max_{(\lambda_1, \lambda_2) \in \Gamma} \frac{P_t^+(\lambda_1, \lambda_2) - E(P_t^+(\lambda_1, \lambda_2))}{\sqrt{Var(P_t^+(\lambda_1, \lambda_2))}}, \quad (11)$$

where $E(P_t^+(\lambda_1, \lambda_2))$, $Var(P_t^+(\lambda_1, \lambda_2))$ respectively are the mean and variance of $P_t(\lambda_1, \lambda_2)$ under H_0 (e.g. for phase-I in-control samples).

Note that the penalty parameters (λ_1, λ_2) detect maximization in equation (11) is generally different under different times t . To emphasize such dependence of time t , we denote the parameter pair that attains the maximization in equation (11) at time t as $(\lambda_{1,t}^*, \lambda_{2,t}^*)$, i.e.,

$$(\lambda_{1,t}^*, \lambda_{2,t}^*) = \arg \max_{(\lambda_1, \lambda_2) \in \Gamma} \frac{P_t^+(\lambda_1, \lambda_2) - E(P_t^+(\lambda_1, \lambda_2))}{\sqrt{Var(P_t^+(\lambda_1, \lambda_2))}}. \quad (12)$$

Thus, the series of the test statistics for the hot-spot at time t is $\tilde{P}_t^+(\lambda_{1,t}^*, \lambda_{2,t}^*)$ where $t = 1 \cdots T$.

With the test statistic available, we design a control chart based on the CUSUM procedure for the following reasons: 1) we are interested in detecting the change with the temporal continuity, therefore, alignment with the objective of CUSUM. 2) In the view of social stability, we want to keep the crime rates at a target value without sudden changes, which makes the CUSUM chart is a naturally better fit.

Specifically, in the CUSUM procedure, we compute the CUSUM statistics recursively

by

$$W_t^+ = \max\{0, W_{t-1}^+ + \tilde{P}_t^+(\lambda_{1,t}^*, \lambda_{2,t}^*) - d\},$$

and $W_{t=0}^+ = 0$, where d is a constant and can be chosen according to the degree of the shift that we want to detect. Next, we set the control limit L as the four times of the standard derivation of $\tilde{P}_t^+(\lambda_{1,t}^*, \lambda_{2,t}^*)(t = 1 \cdots T)$. Finally, whenever $W_t^+ > L$ at some time $t = t^*$, we determine that a temporal hot-spot occurs at time t^* .

4.2 Localize Where and Which the Hot Spot Occur?

After the temporal hot-spot t^* has been detected by the CUSUM control chart in the previous subsection, the next step is to localize where and which crime rate may account for this temporal hot-spot. To do so, we propose to utilize the matrix

$$\hat{\mathbf{h}}_{\lambda_{1,t^*}^*, \lambda_{2,t^*}^*} = \mathbf{B}_h \hat{\boldsymbol{\theta}}_{h, \lambda_{1,t^*}^*, \lambda_{2,t^*}^*}$$

at the declared hot-spot time t^* and the corresponding parameter $\lambda_{1,t^*}^*, \lambda_{2,t^*}^*$ in equation (12). For the numerical computation purpose, it is often easier to directly work with the tensor format of the hot-spot $\hat{\mathbf{h}}_{\lambda_{1,t^*}^*, \lambda_{2,t^*}^*}$, denoted as $\hat{\mathcal{H}}_{h, \lambda_{1,t^*}^*, \lambda_{2,t^*}^*}$, which is a tenor of dimension $n_1 \times n_2 \times T$. If the (i, j, t^*) entry in $\hat{\mathcal{H}}_{h, \lambda_{1,t^*}^*, \lambda_{2,t^*}^*}$ is non-zero, then we declare that there is a hot-spot for the j^{th} crime rate type in the i^{th} state in t^{*th} year.

5 Monte Carlo Simulation

In this section, we conduct simulation studies to evaluate our proposed methodologies by comparison with several benchmark methods in the literature. The structure of this section is as follow. We first present the data generation mechanism for our simulations in Section 5.1, then discuss the performance of hot-spot detection and localization in Section 5.2, and finally investigate the fitness of the global trend background in Section 5.3.

5.1 Generative Model in Simulation

In our simulation, at each time index $t(t = 1 \cdots T)$, we generate a vector \mathbf{y}_t of length $n_1 n_2$ by

$$\mathbf{y}_{i,t} = (\mathbf{B}\boldsymbol{\theta}_t)_i + \delta \mathbb{1}\{t \geq \tau\} \mathbb{1}_i\{i \in S_h\} + \mathbf{w}_{i,t}, \quad (13)$$

where $\mathbf{y}_{i,t}$ denotes the i -th entry in vector \mathbf{y}_t , and $(\mathbf{B}\boldsymbol{\theta}_t)_i$ denotes the i -th entry in vector the $\mathbf{B}\boldsymbol{\theta}_t$. Besides, parameter δ denotes the change magnitude. Here $\mathbb{1}(A)$ is the indicator function, which has the value 1 for all elements of A and the value 0 for all elements not in A , and $\mathbf{w}_{i,t}$ is the i -th entry in the white noise vector whose entries are independent and follow $N(0, 0.1^2)$ distribution.

For the anomaly setup, $\mathbb{1}\{t \geq \tau\}$ indicates that the spatial hot-spots only occur after the temporal hot-spot τ . This ensures that the simulated hot-spot is temporal consistent. The second indicator function $\mathbb{1}_i\{i \in S_h\}$ shows that only those entries whose location index belongs set S_h are assigned as local hot-spots. This ensures that the simulated hot-spot is sparse. Here we assume the change happens at $\tau = 20$ and the spatial hot-spots index set $S_h = \{3, 4, 5, 45, 46, 47, 57, 58, 59, 77, 78, 79, 119, 120, 121, 137, 138, 139\}$.

To match the dimension in the case study, we choose $n_1 = 48, n_2 = 3, T = 50$. For the three terms on the right side of equation (13), they serve for the global trend mean, local sparse anomaly and white noise respectively.

In our simulation, the matrix \mathbf{B} is a fixed B-spline basis with degree of three and ten knots. Note that the B-spline basis is only used in the generative model in simulation to generate data, but is not used in our proposed methodologies.

Moreover, the vector $\boldsymbol{\theta}_t$ is generated by a normal distribution, and we consider the following two scenarios:

- Scenario 1: The global trend background is stationary, in which $\boldsymbol{\theta}_t$ is generated by the normal distribution with mean 1 and standard deviation 0.1.
- Scenario 2: The global trend background is decreasing over time, in which $\boldsymbol{\theta}_t$ is generated by normal distribution with mean 0.95^{t-1} and standard deviation 0.1.

Moreover, in each of these two scenarios, we further consider two subcases, depending on the value of change magnitude δ in (13): one is $\delta = 0.1$ (small shift) and the other is $\delta = 0.5$

(large shift).

5.2 Hot-spot Detection Performance

In this section, we compare the performance of our proposed method (denoted as ‘SSR-tensor’) for detection of hot-spots with some benchmark methods. Specifically, we compare our proposed method with Hotelling T^2 control chart (Qiu, 2013) (denoted as ‘T2’), LASSO-based control chart proposed by Zou and Qiu (2009) (denoted as ‘ZQ LASSO’) and SSD proposed by Yan et al. (2018) (denoted as ‘SSD’). Note that the main difference between our SSR-tensor method and the SSD method in Yan et al. (2018) is the autoregressive or Fussed LASSO penalty in (3) so as to ensure the temporal continuity of the hot-spot.

For the basis choices of our proposed method, to model the spatial structure of the global trend, we choose $B_{m,1}$ as the kernel matrix to describe the smoothness of the background, whose (i, j) entry is of value $\exp\{-d^2/(2c^2)\}$ where d is the distance between the i -th state and j -th state and c is the bandwidth chosen by cross-validation. In addition, we choose identity matrices for the temporal basis and crime type basis since we do not have any prior information. Moreover, we use the identity matrix for the spatial and temporal basis of the hot-spots. For SSD in Yan et al. (2018), we will use the same spatial and temporal basis in order to have a fair comparison.

For evaluation, we will compute the following four criteria: (i) precision, defined as the proportion of detected hot-spots that are true hot-spots; (ii) recall, defined as the proportion of the hot-spots that are correctly identified; (iii) F measure, a single criterion that combines the precision and recall by calculating their harmonic mean; and (iv) the corresponding average run length (ARL_1), a measure on the average detection delay in the special scenario when the change occurs at time $t = 1$. All simulation results below are based on 1000 Monte Carlo simulation replications.

Table 1 and Table 2 report the simulation results of our proposed SSR-tensor method and four other baseline methods. Note that the two baseline methods, PCA and T2, cannot localize the hot-spots, and thus we do not report the corresponding values on the precision, recall, and F-measure. Moreover, in our simulation, if a method fails to detect any temporal hot-spots within the entire $T = 50$ years (recall that the true hot-spot occurs

at time $\tau = 20$), we record its detection delay as 30. Thus, for those methods with the large standard deviation of ARL_1 , it is likely caused by the failure of reporting temporal hot-spots.

From Tables 1 and 2, it is easy to see that our proposed SSR-tensor method achieves the smallest ARL_1 and largest F-measure due to the ability to capture both temporal consistency and spatial sparsity of the hot-spots. This implies that our proposed method not only provides a more immediate alarm when the temporal hot-spots occurs but also gives a more accurate estimation of the hot-spots location when they occur.

Meanwhile, the two baseline methods, SSD and ZQ LASSO, are worse than our proposed SSR-tensor method due to their inability to capture the temporal continuity of the hot-spots, particularly in Scenario 2 (decreasing global trend). The baseline methods, PCA and T2, perform the worst due to their inability to detect the sparse changes. In particular, T2 fails to detect the hot-spots even under the large shift scenario (i.e. ARL_1 is 30). The reason is that T2 is designed based on a multivariate hypothesis test, whose power deteriorates in the high-dimensional setting, which is our case.

methods	large shift $\delta = 0.5$				small shift $\delta = 0.1$			
	precision	recall	F measure	ARL	precision	recall	F measure	ARL
SSR-tensor	0.2714	0.9667	0.6190	1.0003	0.2401	0.9778	0.6089	1.2130
	(0.0171)	(0.0286)	(0.0188)	(0.1026)	(0.0219)	(0.0388)	(0.0283)	(0.3078)
SSD	0.2636	0.9840	0.6238	1.0018	0.2311	0.9300	0.5806	1.7865
	(0.0141)	(0.0292)	(0.0189)	(0.1132)	(0.0553)	(0.2164)	(0.1353)	(0.5693)
ZQ LASSO	0.1351	0.9850	0.5600	2.4178	0.1325	0.8771	0.5048	5.9560
	(0.0180)	(0.0302)	(0.0118)	(1.0097)	(0.0124)	(0.1215)	(0.0586)	(1.7385)
PCA	-	-	-	19.8310	-	-	-	24.4120
	-	-	-	(9.0701)	-	-	-	(10.4709)
T2	-	-	-	30.0000	-	-	-	30.0000
	-	-	-	(0.0000)	-	-	-	(0.0000)

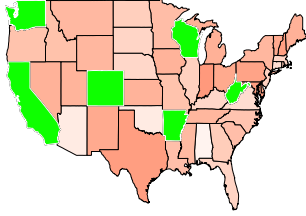
Table 1: Scenario 1 (stationary global trend): Comparison of hot-spot detection under small and large shifts

methods	large shift $\delta = 0.5$				small shift $\delta = 0.1$			
	precision	recall	F measure	ARL	precision	recall	F measure	ARL
SSR-tensor	0.3068	0.9999	0.6534	1.0800	0.2538	0.9833	0.6186	9.0087
	(0.0435)	(0.0001)	(0.0217)	(0.6831)	(0.0155)	(0.0268)	(0.0194)	(5.4261)
SSD	0.2839	0.9944	0.6392	1.4300	0.2298	0.8856	0.5578	12.1600
	(0.0221)	(0.0201)	(0.0180)	(0.8072)	(0.0781)	(0.2981)	(0.1878)	(9.4598)
ZQ LASSO	0.1251	0.9800	0.5556	3.4770	0.0457	0.3609	0.2033	20.7200
	(0.0150)	(0.1175)	(0.0662)	(4.6848)	(0.0607)	(0.4794)	(0.2701)	(12.6450)
PCA	-	-	-	24.3220	-	-	-	21.5380
	-	-	-	(8.8534)	-	-	-	(9.2965)
T2	-	-	-	30.0000	-	-	-	30.0000
	-	-	-	(0.0000)	-	-	-	(0.0000)

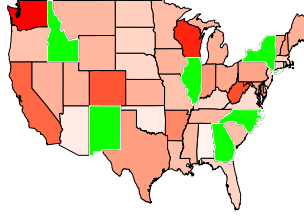
Table 2: Scenario 2 (decreasing global trend): Comparison of hot-spot detection under small and large shifts

In addition, we also visualize our hot-spot detection results in Figure 3. From Figure 3, we can see that our proposed SSR-Tensor method can accurately detect the hot-spot location with the smallest false positive (i.e. red).

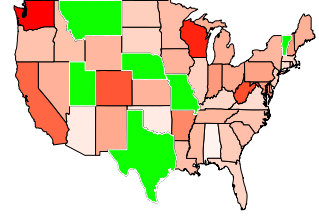
Figure 4 illustrates the trend of the detection delay, ARL_1 , of all methods, as δ changes from 0.1 to 0.5 with the step size of 0.1. From the plot, our proposed SSR-Tensor method (the red curve) has the smaller detection delays than other baseline methods, particularly when there is a decreasing global trend and the magnitude of the hot-spot is small. Also, it is interesting to note that the detection delays of all methods are decreasing as the magnitude of the hot-spot is increasing, which is consistent with our intuition that it is easier to detect larger changes. In addition, note that the PCA method has the largest detection delays since it fails to consider the spatio-temporal correlation and the sparsity of the spatial hot-spots.



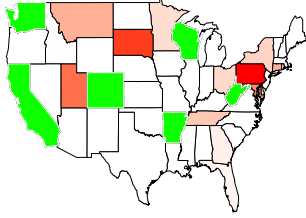
(a) ZQ LASSO in category1



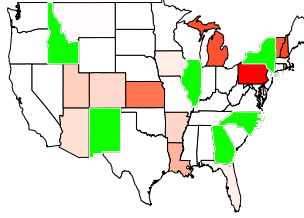
(b) ZQ LASSO in category2



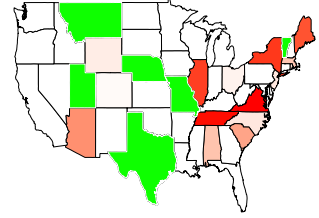
(c) ZQ LASSO in category3



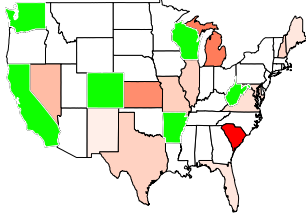
(d) SSD in category1



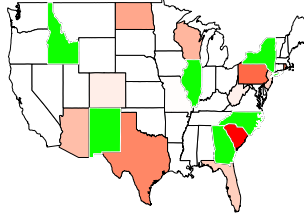
(e) SSD in category2



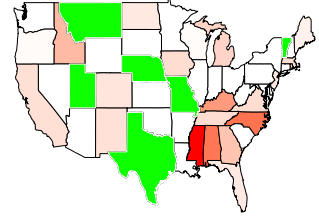
(f) SSD in category3



(g) SSR-Tensor in category1

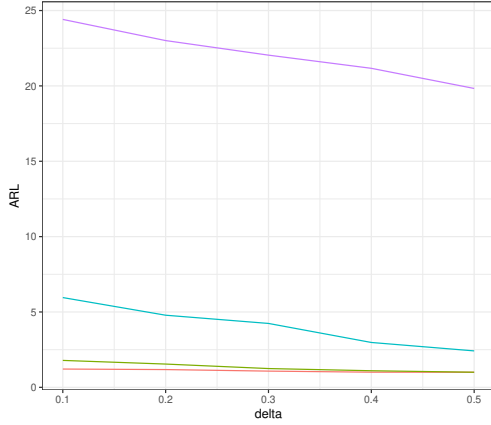


(h) SSR-Tensor in category2

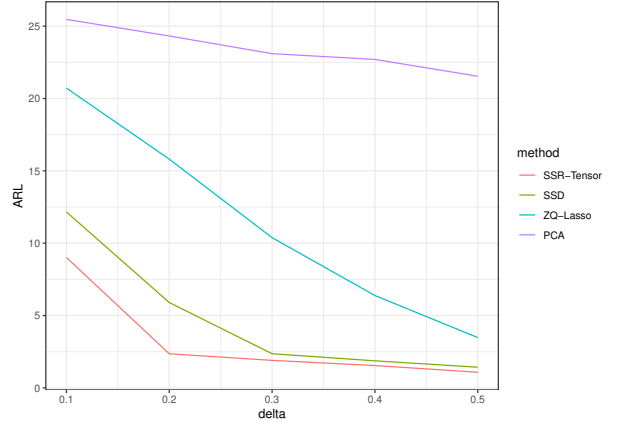


(i) SSR-Tensor in category3

Figure 3: Spatial hot-spot detection performance by ZQ LASSO, SSD and our proposed SSR-Tensor method in Scenario 2 (decreasing global trend) with a large hot-spot of $\delta = 0.5$. Here red is for the falsely detected hot-spots by the algorithm (i.e. false positive), blue refers to the undetected but true hot-spots (i.e. false negative), and green means the detected and true hot-spots (i.e. true positive))



(a) ARL under no global trend



(b) ARL under decreasing global trend

Figure 4: ARL_1 plot under different magnitude δ of the hot-spot

5.3 Background Fitness

In this subsection, we will illustrate that our proposed SSR-tensor has a good estimation for the global trend background. To do this, we compare the Squared-Root of Mean Square Error (SMSE) of the fitness of a global trend mean in Table 3. Here we only compare our proposed method with SSD, since other baseline methods (ZQ LASSO, PCA, and T2) do not discuss how to estimate the global trend background. It is clear from Tables 3 that our proposed SSR-tensor method does better in terms of the background fitness, especially in the scenario 2 (decreasing global trend).

6 Case Study

In this section, we apply our proposed SSR-tensor method to the crime rate dataset described in Section 2. Our proposed method is compared with other benchmarks (the same benchmarks we used in Section 5) from two aspects, one is the performance in the temporal detection of hot-spots (i.e., which year it occurs) and the other is the performance in the localization of the hot-spots (i.e., which state and which type of crime rates may trigger the alarm).

First, we compare the performance of the detection speed of hot-spots. For our proposed SSR-Tensor method, we build a CUSUM control chart utilizing the test statistic in Section

methods	$\delta = 0.1$	$\delta = 0.2$	$\delta = 0.3$	$\delta = 0.4$	$\delta = 0.5$
Scenario 1 (stationary global trend)					
SSR-tensor	0.0279	0.1712	0.1778	0.1873	0.1997
	(0.0024)	(0.0025)	(0.0025)	(0.0024)	(0.0020)
SSD	0.1779	0.1826	0.1928	0.2076	0.2098
	(0.0101)	(0.0052)	(0.0029)	(0.0024)	(0.0023)
Scenario 2 (decreasing global trend)					
SSR-tensor	0.0030	0.0030	0.0030	0.0031	0.0031
	(0.0072)	(0.0068)	(0.0061)	(0.0064)	(0.0060)
SSD	0.2778	0.2725	0.2781	0.2842	0.2602
	(0.0136)	(0.0114)	(0.0143)	(0.0113)	(0.0084)

Table 3: SMSE in two scenarios with different shift

4, which is shown in Figure 5. From this plot, we can see that the hot-spots are detected at 24 – 25-th, 32 – 35-th and 44-th years, i.e, 1989-1990, 1997-2000 and 2009.

For the purpose of comparison, we also apply SSD (Yan et al., 2018), ZQ LASSO (Zou and Qiu, 2009), PCA (De Ketelaere et al., 2015) and T2 (Qiu, 2013) to the crime rate dataset and summarize the performance of the detection of a temporal hot-spot in Table 4. Note that all the temporal changes reported in Table 4 is the first alarm year. Clearly, our proposed SSR-tensor method achieves the fastest detection of the hot-spot compared to all other benchmark methods. Numerically verified in simulation, we can say that it is of quite likely that 1989-1990, 1997-2000 and 2009 are indeed temporal hot-spots, and our proposed SSR-tensor method works well in the crime rate dataset.

methods	SSR-Tensor	SSD	ZQ LASSO	PCA	T2
NO. of year that the first temporal changes	24	30	None	None	None

Table 4: Detection of hot-spot in crime rate dataset

Next, after the detection of hot-spots, we need to further localize the hot-spots in the sense that we need to find out which state and which type of crime rate may lead to the occurrence of a temporal hot-spot. Because the baseline methods, PCA and T2, can

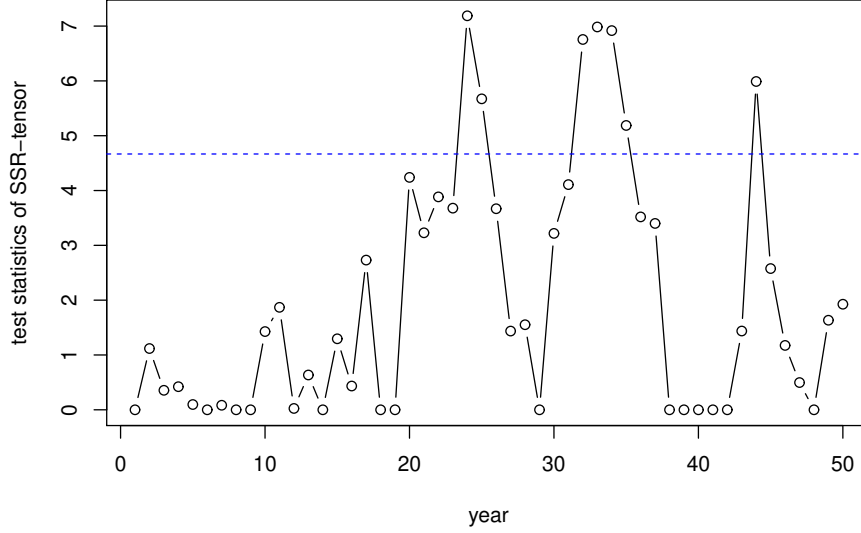


Figure 5: Detection of temporal hot-spot by SSR-Tensor

only realize the detection of temporal changes and ZQ-LASSO fails to detect any temporal changes, we only show the localization of spatial hot-spot by SSR-Tensor and SSD, where the results are visualized in Figure 6.

Compared to SSD, it can be seen that our proposed SSR-tensor method detects more sparse hot-spots, which might be useful to identify the most important hot-spots. As an example, let us consider Kansas, which is declared as a hot-spot in all the three temporal changes year 1989, 1997 and 2009. Figure 7 shows the time series plot of the first type of crime rate in Kansas. The plot shows that, during the decreasing trend of the last 30 years, Kansas experienced some sudden increase, which may cause it to be detected as a spatial hot-spot by SSR-Tensor. Another example is the state of South Carolina, which is declared as a hot-spot in 1989. One possible explanation is that hurricane Hugo makes landfall in South Carolina in September 1989, causing \$7 billion in damage. The hurricane tended to damage people's home and cut their food supply, which possibly leads to an increase in the crime rates.

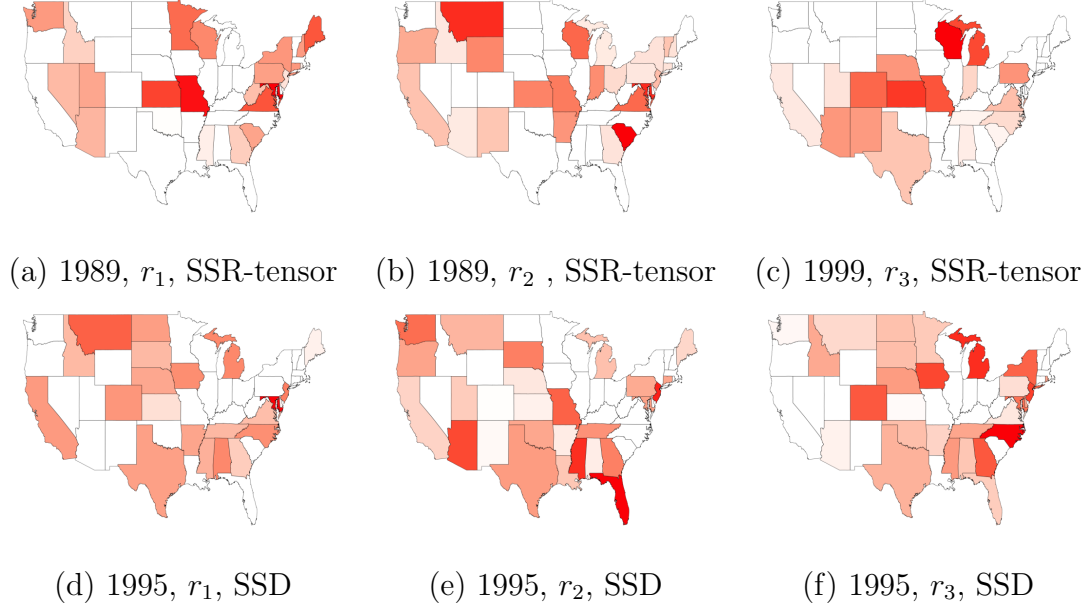


Figure 6: Localization of hot-spot. Top row: three crime rates by our proposed SSR-Tensor method. Bottom row: three crime rates by the SSD. The red color of the states means that, there is an upward shift for this corresponding state and the deeper the color, the larger increase of the rate.

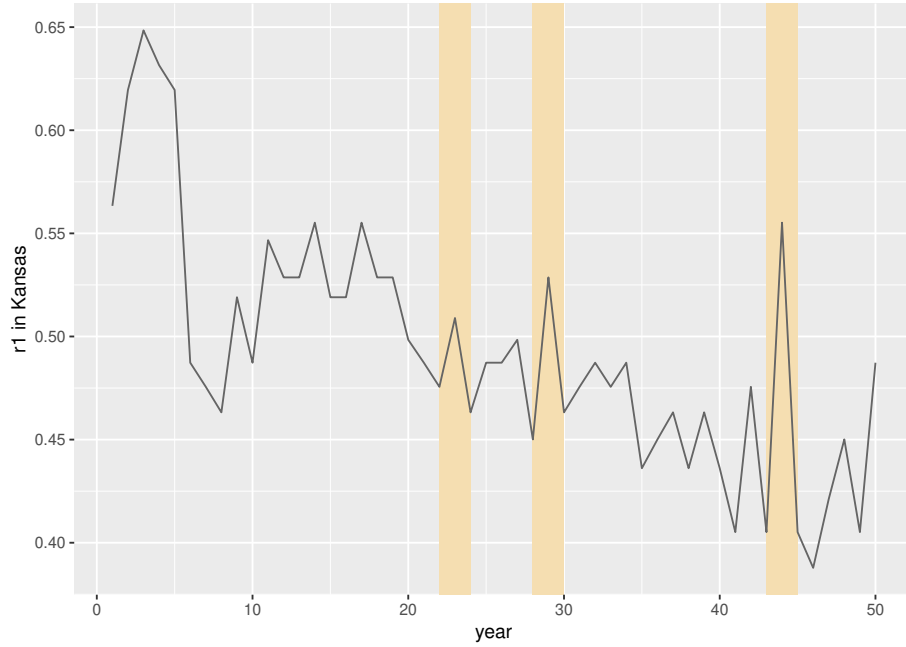


Figure 7: Time series plot of the first type of crime rate in Kansas

7 Conclusion

Hot-spot detection in spatio-temporal data is an important problem in real life. In this paper, we propose the ‘SSR-Tensor’ method for detection of hot-spots in spatio-temporal data. Unlike existing methods for hot-spot detection, which is only workable for scalar or functional data, our proposed SSR-Tensor method is able to decompose the variate pattern of the multi-dimension data into the global trend mean, local hot-spots and residuals. The estimation of hot-spot is solved by optimizing the sum of residuals with two penalty terms, which controls the sparsity of the hot-spots and the temporal consistency of the hot-spots, respectively.

To efficiently solve the above-mentioned high-dimensional optimization problems, we first reduce the unknown parameters and then simplify the generalized LASSO problem into the regular LASSO problem where many well-known LASSO algorithms can be used. We chose the FISTA algorithm in our paper because it currently has the fastest convergence rate up. We compare our proposed SSR-Tensor method with other benchmarks in terms of detection accuracy, computational time and background fitness. Based on Monte Carlo simulations and the case study of the crime rate dataset, we conclude that, overall our proposed SSR-Tensor method outperforms other benchmarks. While the classical statistical process control (SPC) or sequential change-point detection problems have been studied for several decades, research on the hot-spot of tensor data is rather limited, mainly due to computational complexity and sparsity of hot-spots. Clearly, there are many opportunities to improve the algorithms and methodologies. For instance, it will be interesting to study the relationship between our proposed SSR-Tensor method and the autoregressive model. Moreover, in this paper, we specify the tensor basis, and then investigate its performance on the detection and localization of the hot-spot. It will be useful to investigate the robustness effects of different tensor bases. Finally, further research direction includes hot-spot detection problems from more complicated data set and broad real-world applications.

8 Appendix

8.1 Proof of Fast Calculation of \mathbf{y}^* via Tensor Algebra

Proof.

$$\begin{aligned}
\mathbf{y}^* &= [\mathbf{I} - \mathbf{B}_m(\mathbf{B}'_m \mathbf{B}_m)^{-1} \mathbf{B}'_m] \mathbf{y} \\
&= \mathbf{y} - \mathbf{B}_m((\mathbf{B}'_{m,s} \otimes \mathbf{B}'_{m,r} \otimes \mathbf{B}'_{m,t})(\mathbf{B}_{m,s} \otimes \mathbf{B}_{m,r} \otimes \mathbf{B}_{m,t}))^{-1} \mathbf{B}'_m \mathbf{y} \\
&= \mathbf{y} - \mathbf{B}_m((\mathbf{B}'_{m,s} \mathbf{B}_{m,s}) \otimes (\mathbf{B}'_{m,r} \mathbf{B}_{m,r}) \otimes (\mathbf{B}'_{m,t} \mathbf{B}_{m,t}))^{-1} \mathbf{B}'_m \mathbf{y} \\
&= \mathbf{y} - \mathbf{B}_m((\mathbf{B}'_{m,s} \mathbf{B}_{m,s})^{-1} \otimes (\mathbf{B}'_{m,r} \mathbf{B}_{m,r})^{-1} \otimes (\mathbf{B}'_{m,t} \mathbf{B}_{m,t})^{-1}) \mathbf{B}'_m \mathbf{y} \\
&= \mathbf{y} - (\mathbf{B}_{m,s}(\mathbf{B}'_{m,s} \mathbf{B}_{m,s})^{-1} \mathbf{B}'_{m,s}) \otimes (\mathbf{B}_{m,r}(\mathbf{B}'_{m,r} \mathbf{B}_{m,r})^{-1} \mathbf{B}'_{m,r}) \otimes (\mathbf{B}_{m,t}(\mathbf{B}'_{m,t} \mathbf{B}_{m,t})^{-1} \mathbf{B}'_{m,t}) \mathbf{y} \\
&= \mathbf{y} - \mathcal{Y} \times_1 (\mathbf{B}_{m,s}(\mathbf{B}'_{m,s} \mathbf{B}_{m,s})^{-1} \mathbf{B}'_{m,s}) \times_2 (\mathbf{B}_{m,r}(\mathbf{B}'_{m,r} \mathbf{B}_{m,r})^{-1} \mathbf{B}'_{m,r}) \times_3 (\mathbf{B}_{m,t}(\mathbf{B}'_{m,t} \mathbf{B}_{m,t})^{-1} \mathbf{B}'_{m,t})
\end{aligned}$$

□

8.2 Proof of Proposition 2

Proof. By introducing matrix $\tilde{\mathbf{D}}$, we change variables to $\hat{\boldsymbol{\beta}} = (\hat{\boldsymbol{\beta}}_1, \hat{\boldsymbol{\beta}}_2) = \tilde{\mathbf{D}} \boldsymbol{\theta}_{h,0,\lambda_2}$. Accordingly, $\|\mathbf{D} \boldsymbol{\theta}_{h,0,\lambda_2}\|_1 = \|\boldsymbol{\beta}_1\|_1$ because the rows in matrix A are orthogonal to those in matrix \mathbf{D} . Besides, $\mathbf{X} \boldsymbol{\theta}_{h,0,\lambda_2} = \mathbf{X} \tilde{\mathbf{D}}^{-1} \boldsymbol{\beta} = \mathbf{X}_1 \boldsymbol{\beta}_1 + \mathbf{X}_2 \boldsymbol{\beta}_2$. Therefore, we can rewrite equation (6) as.

$$\arg \min_{\boldsymbol{\theta}_{h,\lambda_1,\lambda_2}} \|\mathbf{y}^* - (\mathbf{X}_1 \boldsymbol{\beta}_1 + \mathbf{X}_2 \boldsymbol{\beta}_2)\|_2^2 + \lambda_2 \|\boldsymbol{\beta}_1\|_1 \quad (14)$$

By taking derivative to $\boldsymbol{\beta}_2$, we have

$$\boldsymbol{\beta}_2 = (\mathbf{X}'_2 \mathbf{X}_2)^{-1} \mathbf{X}'_2 (\mathbf{y} - \mathbf{X}_1 \boldsymbol{\beta}_1). \quad (15)$$

By plugging in equation (15), we can rewrite equation (14) as that shown in equation (8). There are lots of R package available for solving lasso, such as *LARS* and *glmnet*, from which we can back-transform to get the generalized lasso solution $\hat{\boldsymbol{\theta}}_{h,0,\lambda_2} = \tilde{\mathbf{D}}^{-1} \hat{\boldsymbol{\beta}}$.

□

References

- Bakshi, B. R. (1998). Multiscale pca with application to multivariate statistical process monitoring. *AIChE journal*, 44(7):1596–1610.
- Beck, A. and Teboulle, M. (2009). A fast iterative shrinkage-thresholding algorithm for linear inverse problems. *SIAM journal on imaging sciences*, 2(1):183–202.
- Call, M. A. and Voss, P. R. (2016). Spatio-temporal dimensions of child poverty in america, 1990–2010. *Environment and Planning A*, 48(1):172–191.
- De Ketelaere, B., Hubert, M., and Schmitt, E. (2015). Overview of pca-based statistical process-monitoring methods for time-dependent, high-dimensional data. *Journal of Quality Technology*, 47(4):318–335.
- Diggle, P. J. (2013). *Statistical analysis of spatial and spatio-temporal point patterns*. CRC Press.
- Elhorst, J. P. (2014). Spatial panel data models. In *Spatial econometrics*, pages 37–93. Springer.
- Hamilton, J. D. (1994). *Time series analysis*, volume 2. Princeton university press Princeton, NJ.
- Hannan, E. J. and Quinn, B. G. (1979). The determination of the order of an autoregression. *Journal of the Royal Statistical Society. Series B (Methodological)*, pages 190–195.
- Hawkins, D. M. (1993). Regression adjustment for variables in multivariate quality control. *Journal of Quality Technology*, 25(3):170–182.
- Hu, K. and Yuan, J. (2009). Batch process monitoring with tensor factorization. *Journal of Process Control*, 19(2):288–296.
- Kolda, T. G. and Bader, B. W. (2009). Tensor decompositions and applications. *SIAM review*, 51(3):455–500.

- Lai, T. L. and Lim, J. (2015). Asymptotically efficient parameter estimation in hidden markov spatio-temporal random fields. *Statistica Sinica*, pages 403–421.
- Lan, H., Zhou, C., Wang, L., Zhang, H., and Li, R. (2004). Landslide hazard spatial analysis and prediction using gis in the xiaojiang watershed, yunnan, china. *Engineering geology*, 76(1-2):109–128.
- Li, Z., Sergin, N. D., Yan, H., Zhang, C., and Tsung, F. (2019). Tensor completion for weakly-dependent data on graph for metro passenger flow prediction. *arXiv preprint arXiv:1912.05693*.
- Lichstein, J. W., Simons, T. R., Shriner, S. A., and Franzreb, K. E. (2002). Spatial autocorrelation and autoregressive models in ecology. *Ecological monographs*, 72(3):445–463.
- Liu, J., Yuan, L., and Ye, J. (2010). An efficient algorithm for a class of fused lasso problems. In *Proceedings of the 16th ACM SIGKDD international conference on Knowledge discovery and data mining*, pages 323–332. ACM.
- Liu, R. Y. (1995). Control charts for multivariate processes. *Journal of the American Statistical Association*, 90(432):1380–1387.
- Louwerse, D. and Smilde, A. (2000). Multivariate statistical process control of batch processes based on three-way models. *Chemical Engineering Science*, 55(7):1225–1235.
- Paynabar, K., Jin, J., and Pacella, M. (2013). Monitoring and diagnosis of multichannel nonlinear profile variations using uncorrelated multilinear principal component analysis. *Iie transactions*, 45(11):1235–1247.
- Paynabar, K., Zou, C., and Qiu, P. (2016). A change-point approach for phase-i analysis in multivariate profile monitoring and diagnosis. *Technometrics*, 58(2):191–204.
- Qiu, P. (2013). *Introduction to statistical process control*. Chapman and Hall/CRC.
- Reynolds, K. and Madden, L. (1988). Analysis of epidemics using spatio-temporal autocorrelation. *Phytopathology*, 78(2):240–246.

- Šaltytė Benth, J. and Šaltytė, L. (2011). Spatial-temporal model for wind speed in lithuania. *Journal of Applied Statistics*, 38(6):1151–1168.
- Tibshirani, R. J., Taylor, J., et al. (2011). The solution path of the generalized lasso. *The Annals of Statistics*, 39(3):1335–1371.
- Tran, L., Navasca, C., and Luo, J. (2012). Video detection anomaly via low-rank and sparse decompositions. In *2012 Western New York Image Processing Workshop*, pages 17–20. IEEE.
- Yan, H., Paynabar, K., and Shi, J. (2014). Image-based process monitoring using low-rank tensor decomposition. *IEEE Transactions on Automation Science and Engineering*, 12(1):216–227.
- Yan, H., Paynabar, K., and Shi, J. (2017). Anomaly detection in images with smooth background via smooth-sparse decomposition. *Technometrics*, 59(1):102–114.
- Yan, H., Paynabar, K., and Shi, J. (2018). Real-time monitoring of high-dimensional functional data streams via spatio-temporal smooth sparse decomposition. *Technometrics*, 60(2):181–197.
- Yu, K., He, L., Philip, S. Y., Zhang, W., and Liu, Y. (2019). Coupled tensor decomposition for user clustering in mobile internet traffic interaction pattern. *IEEE Access*, 7:18113–18124.
- Zhang, C., Yan, H., Lee, S., and Shi, J. (2018). Multiple profiles sensor-based monitoring and anomaly detection. *Journal of Quality Technology*, 50(4):344–362.
- Zhu, J., Huang, H.-C., and Wu, J. (2005). Modeling spatial-temporal binary data using markov random fields. *Journal of Agricultural, Biological, and Environmental Statistics*, 10(2):212.
- Zou, C., Ning, X., and Tsung, F. (2012). Lasso-based multivariate linear profile monitoring. *Annals of Operations Research*, 192(1):3–19.

- Zou, C. and Qiu, P. (2009). Multivariate statistical process control using lasso. *Journal of the American Statistical Association*, 104(488):1586–1596.
- Zou, C., Tsung, F., and Wang, Z. (2008). Monitoring profiles based on nonparametric regression methods. *Technometrics*, 50(4):512–526.